Transactions of Tianjin University (2021) 27:331–337
https://doi.org/10.1007/s12209-021-00292-w

RESEARCH ARTICLE

Simultaneously Enhanced Activity and Selectivity for C(sp^3)–H Bond Oxidation Under Visible Light by Nitrogen Doping

Tingting Hou[1] · Zhuyan Gao[2,3] · Jian Zhang[2] · Nengchao Luo[2] · Feng Wang[2]

Received: 27 March 2021 / Revised: 6 April 2021 / Accepted: 28 April 2021 / Published online: 1 June 2021

Abstract

Selective oxidation of saturated C(sp^3)–H bonds in hydrocarbon to target chemicals under mild conditions remains a significant but challenging task because of the chemical inertness and high dissociation energy of C(sp^3)–H bonds. Semiconductor photocatalysis can induce the generation of holes and oxidative radicals, offering an alternative way toward selective oxidation of hydrocarbons under ambient conditions. Herein, we constructed N-doped TiO_2 nanotubes (N-TNTs) that exhibited remarkable activity and selectivity for toluene oxidation under visible light, delivering the conversion of toluene and selectivity of benzaldehyde of 32% and > 99%, respectively. Further mechanistic studies demonstrated that the incorporation of nitrogen induced the generation of N-doping level above the O 2*p* valance band, directly contributing to the visible-light response of TiO_2. Furthermore, hydroxyl radicals generated by photogenerated holes at the orbit of O 2*p* were found to be unselective for the oxidation of toluene, affording both benzaldehyde and benzoic acid. The incorporation of nitrogen was able to inhibit the generation of hydroxyl radicals, terminating the formation of benzoic acid.

Keywords Visible light · c(sp^3) · H oxidation · N-doped TiO_2 · Selectivity · Benzaldehyde

Introduction

Selective oxidation of hydrocarbon to produce high-value-added oxygenates is being pursued in both fundamental and applied chemistry [1–5]. Unfortunately, because of the chemical inertness and high bond dissociation energy (355–439 kJ/mol) of C(sp^3)–H bonds, the activation of C(sp^3)–H bonds is regarded as the most critical step during the oxidation of hydrocarbon. Thus, the oxidation of hydrocarbon is usually operated under harsh reaction conditions with high temperature, pressure, or corrosive reagents, resulting in adverse effects on the environment as well as high energy costs [6–8]. Free radicals and holes are known to have a superior ability to directly initiate the activation of C(sp^3)–H bonds, even under moderate conditions. Thus, semiconductor photocatalysis, which can induce the generation of free radicals and holes, offers an alternative way toward selective oxidation of hydrocarbons under ambient conditions [4, 9–20].

As a widely used semiconductor, TiO_2 has attracted extensive attention for alkane oxygenation [21–25]. However, because of its large band gap, the corresponding reactions are usually operated under the irradiation of ultraviolet (UV) light, which only accounts for approximately 4% of the total solar spectrum. Furthermore, a wide range of radicals is able to be initiated at the valence or conduction band of TiO_2, generally resulting in a high degree of non-selectivity and thus a wide product distribution [26]. Thanks to the efforts from other groups, various strategies (including varying crystal structure, constructing hybrid structures, and surface decoration) have been adopted to realize the selective oxidation of hydrocarbon over TiO_2-based catalysts under visible light [27–29]. For example, Schmuki et al. [26] discovered that the variation of crystal structure from anatase to rutile was able to increase the selectivity of benzaldehyde

Tingting Hou and Zhuyan Gao contributed equally to this work.

✉ Feng Wang
wangfeng@dicp.ac.cn

[1] School of Chemistry and Chemical Engineering, South China University of Technology, Guangzhou 510640, China

[2] State Key Laboratory of Catalysis, Dalian National Laboratory for Clean Energy, Dalian Institute of Chemical Physics, Chinese Academy of Sciences, Dalian 116023, China

[3] University of Chinese Academy of Sciences, Beijing 100049, China

from 26.55 to 75.66%. Further doping Ru atoms into rutile elevated the selectivity of benzaldehyde to 89.07% while achieving the complete suppression of benzoic acid under the same reaction conditions. In addition, Yin et al. [30] loaded TiO_2 nanoparticles on a Bi_2MoO_6 sheet to fabricate TiO_2/Bi_2MoO_6 heterostructures that were used to selectively oxidize toluene to benzaldehyde via visible-light excitation at a toluene conversion of 1.6%. And Yuan et al. [31] applied surface-chlorinated $BiOBr/TiO_2$ for photocatalytic oxidation of toluene; the generated chlorine radicals under irradiation of visible light were highly efficient for C(sp^3)–H cleavage. Although great progress has been achieved in improving photocatalytic activity, developing a simple way to synchronously achieve high activity and high selectivity of TiO_2-based catalysts during hydrocarbon oxidation under irradiation with visible light is still urgently desired.

Herein, we successfully constructed a photocatalyst of N-doped TiO_2 nanotubes (N-TNTs) by a simple solvothermal method using NH_4Cl as the nitrogen source. The as-obtained N-TNTs exhibited remarkable activity and selectivity for the selective activation of C(sp^3)–H under visible-light irradiation, delivering the conversion of toluene and selectivity of benzaldehyde of 32% and > 99%, respectively. Further mechanistic studies demonstrated that the incorporation of nitrogen induced the generation of N-doping level above the O 2*p* valance band, directly contributing to the visible-light response of TiO_2. Furthermore, the hydroxyl radical generated by the holes at the orbit of O 2*p* could result in the unselective oxidation of toluene to benzaldehyde and benzoic acid. The incorporation of nitrogen was found to be able to inhibit the generation of hydroxyl radicals, terminating the formation of benzoic acid.

Results and Discussion

To produce the photocatalyst, TiO_2 powders were hydrothermally treated in 10 M of NaOH aqueous solution at 150 °C for 12 h, followed by washing with 0.1 M of dilute HNO_3 solution and deionized water. After being dried, the obtained white powders held the nanotubular structure with the outer and inner diameters of 8 nm and 5 nm, respectively; the material was named as H-TNTs (Fig. 1a). To introduce N species into the sample, H-TNTs were treated with NH_4Cl solution at 120 °C for 8 h. This sample was named as NH_4^+-TNTs. As shown in Fig. 1b, the effect of the

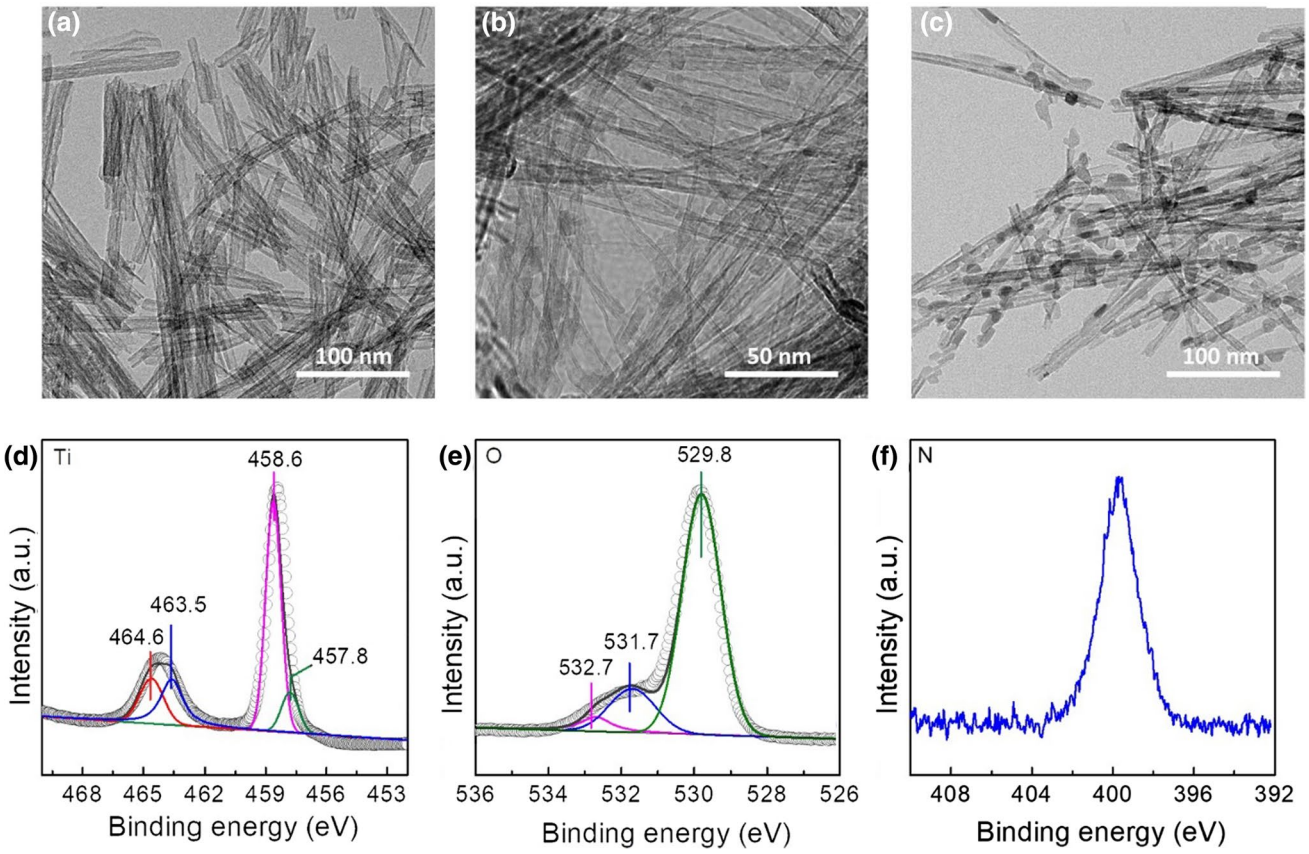

Fig. 1 Characterization of the as-obtained samples. TEM images of **a** H-TNTs, **b** NH_4^+-TNTs, and **c** N-TNTs. XPS spectra of **d** Ti 2*p*, **e** O1*s*, and **f** N1*s* for N-TNTs

treatment with NH_4Cl on morphology was negligible. Obviously, the NH_4^+-TNTs exhibited a nanotubular structure with similar diameters to those of the H-TNTs (Fig. 1b). Finally, N-doped TiO_2 nanotubes (N-TNTs) were obtained via the calcination of NH_4^+-TNTs with air at 400 °C. As shown in transmission electron microscopy (TEM) images, N-TNTs inherited the nanotubular structures of the H-TNTs and were accompanied by some nanoparticles because of the partial sintering (Fig. 1c). To analyze the structure of the particles, we also conducted HRTEM measurements. As shown in Fig. S1, the HRTEM image of N-TNTs displayed fringes with an interplanar spacing of 0.35 nm corresponding to the crystal planes (101) of TiO_2. Thus, the particles observed in the TEM images are N-TiO_2 nanoparticles because of the partial sintering, no impurities. The Brunauer–Emmett–Teller (BET) surface areas of H-TNTs, NH_4^+-TNTs, and N-TNTs were also measured to be 335, 354, and 283 m^2/g, respectively (Fig. S2 and Table S1). The decreased BET surface area of N-TNTs compared with those of H-TNTs and NH_4^+-TNTs was attributed to the partial sintering during calcination. Figure S3 shows X-ray diffraction (XRD) patterns of all the samples. The raw TiO_2 powders presented a well-crystallized anatase structure with the representative peak of [101] diffraction at the scattering angle (2θ) of 25.28°. The XRD peaks for H-TNTs, NH_4^+-TNTs, and N-TNTs were found to still be indexed to the anatase phase except for being less distinct and wider. This difference was attributed to the thin walls of H-TNTs, NH_4^+-TNTs, and N-TNTs, which are comprised of just several crystalline layers [32].

To further characterize the electronic properties of N–TNTs, we conducted X-ray photoelectron spectroscopy (XPS) measurements. As shown in the XPS spectrum of Ti 2p (Fig. 1d), four main constituent peaks were fitted: the two peaks at 458.6 eV and 464.6 eV correspond to Ti^{4+}, and the two peaks at 457.8 eV and 463.5 eV correspond to Ti^{3+}. As for XPS spectrum of O 1*s* (Fig. 1e), three peaks centered at 529.8, 531.7, and 532.7 eV were ascribed to the lattice oxygen, OH species, and oxygen atoms near the oxygen vacancy, respectively [33]. N 1*s* XPS measurement for N-TNTs was also carried out. As shown in Fig. 1f, an obvious peak at 400 eV attributed to interstitial N species [34–36] was observed. The electron spin resonance (ESR) technique, unlike other spectroscopic techniques, presents a unique sensibility that allows one to detect paramagnetic species, even at very low concentrations, such as those typical of N-doped TiO_2 systems. These species are characterized by comparing the observed ESR hyperfine coupling constants with the computed values for structural models of substitutional and interstitial nitrogen impurities. As shown in Fig. S4, the signals of ESR were fitted into a typical rhombic g ($g_1 = 2.0054$, $g_2 = 2.0036$, and $g_3 = 2.0030$). This result clearly indicates the presence of a single N atom in the species. The absence of H hyperfine lines in the spectrum rules out the presence of NH_x paramagnetic fragments [37]. This result implies the successful introduction of N into N-TNTs. As a result, the N-doped TiO_2 nanotubes with surface defects (Ti^{3+} and oxygen vacancies) were successfully constructed by employing NH_4Cl as the N source.

The photocatalytic performance of the as-obtained N-TNTs was evaluated toward aerobic oxidation of toluene. Each reaction was performed under 1 atm of O_2 at 25 °C with CH_3CN as the solvent. Figure 2a illustrates the activity and selectivity for all of the catalysts under the irradiation of monochromatic light from 9 W LEDs. When the reaction was catalyzed by anatase, H-TNTs, and NH_4^+-TNTs under the irradiation of 455-nm light, no products were observed (Table S2, entries 1–3). After switching the wavelength of the monochromatic light to 365 nm, anatase, H-TNTs, and NH_4^+-TNTs exhibited photocatalytic activity toward the oxidation of toluene with the generation of benzaldehyde and benzoic acid. As shown in Fig. 2a, the selectivity of benzoic acid for anatase, H-TNTs, and NH_4^+-TNTs was determined to be 48%, 64%, and 26%, respectively. As for N-TNTs, visible light was able to trigger the oxidation of toluene with the yield and selectivity of benzaldehyde of 32% and > 99%, respectively (Fig. 2a). More importantly, this remarkable activity and selectivity of N-TNTs were maintained over 12 h, even under AM 1.5 G illumination (Fig. 2b). This result was comparable to findings in recent reports (Table S3). Interestingly, the selectivity of benzaldehyde over N-TNTs sharply declined to 35% under irradiation of 365-nm light (Table S2, entry 4). As a comparison, the reaction did not proceed in the absence of catalyst or light, indicative of a photocatalytic process (Table S2, entries 5–6). Note that no CO_2 was detected in the gaseous phase for all the cases. To further evaluate the light utilization efficiency, the wavelength-dependent apparent quantum efficiencies (AQEs) of N-TNTs were determined by measuring the conversion of toluene under various monochromatic light irradiation conditions (Fig. 2c). The AQEs were found to be well matched to the absorption capabilities in the full spectrum. Specifically, the AQE at 410 nm was determined to be 4.65%. In addition, the stability of N-TNTs was also studied by performing successive rounds of reaction. As revealed in Fig. S5, almost 94% of the original reaction activity was preserved after five rounds. We also characterized the structure of the recovered N-TNTs by XRD. As shown in Fig. S6, the XRD patterns of the sample were indexed to an anatase phase. Thus, N-TNTs exhibited high stability during the catalytic process. Figure 2d shows the catalytic performance of the oxidation of C–H bonds in alkyl aromatics using N-TNTs as the catalyst under the irradiation of 455-nm LEDs for 12 h. For all alkyl aromatics, the selective oxidation of the C_α–H bond was observed over N-TNTs with the generation of corresponding aldehydes or ketones. As a result, N-TNTs exhibited excellent applicability in selectively photocatalytic

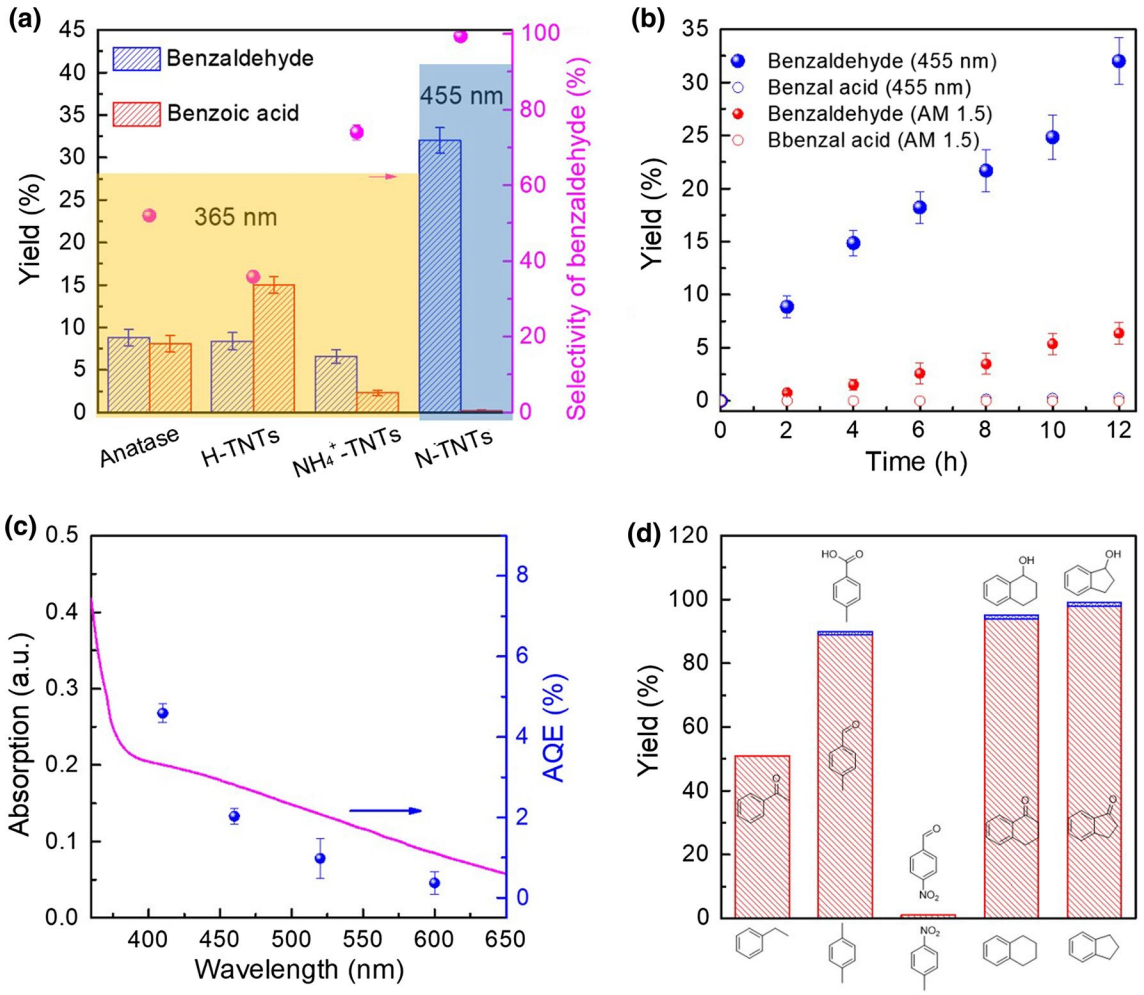

Fig. 2 **a** Photocatalytic oxidation of toluene over anatase, H-TNTs, NH_4^+-TNTs, and N-TNTs. **b** Time courses of photocatalytic oxidation of toluene over N-TNTs under irradiation of 455-nm LEDs and AM 1.5 G. **c** Calculated AQEs for photocatalytic oxidation of toluene over N-TNTs under monochromatic light irradiation. **d** Substrates scope experiments over N-TNTs

oxidation of the C–H bond to produce the corresponding aldehydes or ketones.

To quantify the remarkable activity of N-TNTs in the oxidation of C–H bonds under visible light, we investigated the optical and electronic structures. Figure 3a shows the ultraviolet–visible diffuse reflectance spectra (UV–Vis DRS) of these catalysts. Obviously, no significant absorption exists in the visible-light region for TiO_2 because of its wide band gap (~3.2 eV). As for H-TNTs, the absorption edge was located at approximately 370 nm. No significant difference was observed between NH_4^+-TNTs and H-TNTs, indicating the nitrogen atom was not incorporated into the matrix of the TiO_2 nanotubes. With regard to N-TNTs, a significant amount of absorption in the visible-light region was observed, implying that the doping of nitrogen atoms directly contributed to the visible-light response of N-TNTs [38]. Furthermore, the band gaps of H-TNTs and N-TNTs were determined to be 3.31 and 2.75 eV, respectively, according to the transformed Kubelka–Munk function (Fig. S7). In addition, the incorporation of nitrogen atom was able to lower the recombination rate of photo-induced electron–hole pairs, thereby improving the photocatalytic activity of N-TNTs toward oxidation of toluene. This point was well verified by photoluminescence (PL) spectroscopy, where N-TNTs possessed the lowest PL intensity compared with anatase, H-TNTs, and NH_4^+-TNTs (Fig. 3b).

To further clarify the origin of remarkable photocatalytic selectivity for N-TNTs, we explored the catalytic mechanism in detail by taking the oxidation of toluene as an example. As shown in Fig. 3c, replacing pure O_2 with air depressed the yield of benzaldehyde from 32 to 16%. When the reaction was conducted under pure Ar, nearly no detectable oxidative products were observed. These results indicate that O_2 was involved in the photocatalytic oxidation of toluene. Furthermore, we investigated the active species for N-TNTs in photocatalytic oxidation of the C–H bond in detail. The

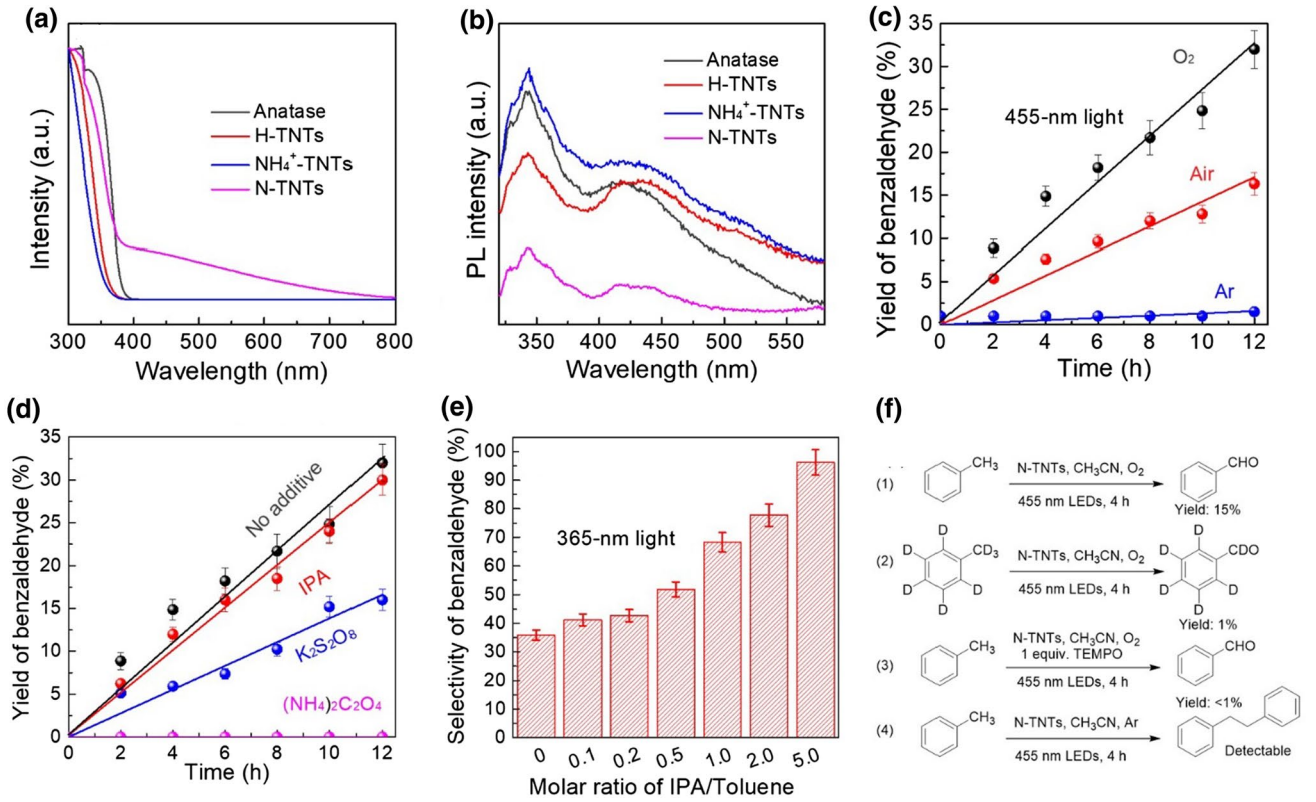

Fig. 3 **a** Diffuse reflectance UV–Vis of the as-obtained samples. **b** PL spectra at the excitation wavelength of 300 nm for the as-obtained samples. Effects of **c** reaction atmosphere, **d** scavenges, and **e** different dots of IPA on the photocatalytic oxidation of toluene over N-TNTs. **f** Control experiment

scavenge measurements were conducted under the irradiation of 455-nm LEDs to identify the active species in the catalytic reactions, where $K_2S_2O_8$, isopropyl alcohol (IPA), and ammonium oxalate were used to selectively eliminate electrons (e^-), hydroxyl radicals ($^\bullet$OH), and holes (h^+), respectively. As shown in Fig. 3d, a total quenching toward the photocatalytic oxidation of toluene was observed in the presence of ammonium oxalate, while IPA was found to have little influence. The scavenging of $K_2S_2O_8$ depressed the yield of benzaldehyde from 32 to 16%. Thus, electrons and holes were regarded as the active species in the generation of benzaldehyde from photocatalytic oxidation of toluene. As for N-TNTs, switching the light wavelength from 455 to 365 nm decreased the selectivity of benzaldehyde to 35% (Table S2). To our delight, adding IPA further inhibited the production of benzoic acid. As shown in Fig. 3e, the selectivity of benzaldehyde reached 96% when adding five equivalents of IPA into the reaction. As mentioned above, the presence of IPA was able to sweep $^\bullet$OH generated during the reaction. Thus, we speculate that hydroxyl radicals were produced under the excitation of ultraviolet light, resulting in the formation of benzoic acid. Furthermore, to elucidate the reaction mechanism, we conducted some control experiments (Fig. 3f). When employing deuterium-labeling toluene (toluene-d6) as the substrate, the yield of benzaldehyde decreased from 15 to 1% under the same reaction conditions (Fig. 3f). This primary kinetic isotope effect (KIE) showed that the benzyl C–H bond oxidation was the rate-determining step. Furthermore, when tetra-methylpiperidine N-oxide (TEMPO), highly selective for carbon-centered radicals [39], was added into the reaction system, the activity was almost completely lost. In addition, after replacing the reaction atmosphere of O_2 with pure Ar, bibenzyl was observed (Fig. S8). Accordingly, we assign a carbon-centered radical as the reaction intermediate during the photocatalytic oxidation of toluene over N-TNTs.

Based on all the above results, we propose the tentative reaction mechanism depicted in Fig. 4. The incorporation of the N element into TiO_2 upward shifted the VB edge via the generation of an N-doping level above the O 2*p* valance band. The N-doping also converted Ti^{4+} species to Ti^{3+} species by charge compensation. The 3d orbital of Ti^{3+} species in TiO_2 served as a donor with energy below the conduction band. Both of these cases contributed to the visible-light response of TiO_2. More importantly, the upward shift of the VB edge was able to inhibit the generation of $^\bullet$OH. As a result, under visible-light irradiation, the photogenerated holes removed a hydrogen ion from benzylic carbon

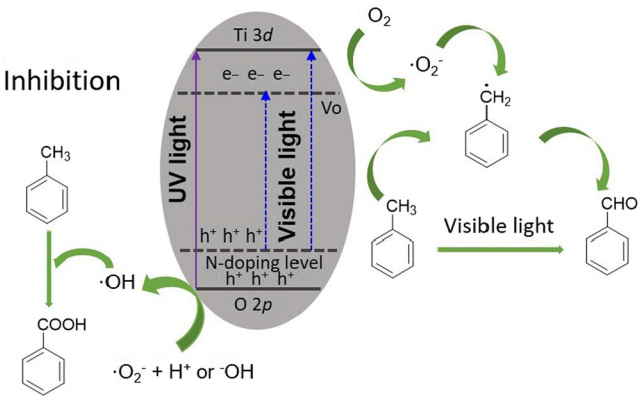

Fig. 4 Proposed mechanism

to generate an alkyl radical. The photogenerated electron was then transferred to O_2, producing a superoxide anion radical. The alkyl radical reacted with superoxide to produce hydroperoxide. Next, the hydroperoxide was converted to benzaldehyde. In the case of pristine TiO_2, photogenerated carriers were generated only under the irradiation of UV light. The photogenerated holes located at the orbit of O 2*p* were able to generate hydroxyl radicals, which further induced the formation of benzoic acid.

Conclusions

In conclusion, we successfully constructed a photocatalyst of N-TNTs toward toluene oxidation under visible light by a simple solvothermal method with NH_4Cl as the nitrogen source, delivering the conversion of toluene and selectivity of benzaldehyde of 32% and > 99%, respectively. Further mechanistic studies demonstrated that the incorporation of nitrogen induced the generation of N-doping level above the O 2*p* valance band, directly contributing to the visible-light response of TiO_2. Furthermore, the hydroxyl radical generated by the holes at the orbit of O 2*p* could result in the unselective oxidation of toluene to benzaldehyde and benzoic acid. The incorporation of nitrogen was able to inhibit the generation of hydroxyl radicals, thereby terminating the formation of benzoic acid. This work provides not only a strategy for developing efficient photocatalysts but also potentially a pathway toward greener industrial processes, especially for temperature-sensitive synthesis.

Supplementary Information The online version contains supplementary material available at https://doi.org/10.1007/s12209-021-00292-w.

Acknowledgements This work was supported by the National Natural Science Foundation of China (Nos. 22025206, 21991094) supported by the Ministry of Science and Technology of the People's Republic of China (No. 2018YFE0118100), the CAS-NSTDA Joint Research Project (No. GJHZ2075), Dalian Science and Technology Innovation Fund (No. 2019J11CY009).

References

1. Laudadio G, Deng YC, van der Wal K et al (2020) C(sp^3)–H functionalizations of light hydrocarbons using decatungstate photocatalysis in flow. Science 369(6499):92–96
2. Xiong LQ, Tang JW (2021) Strategies and challenges on selectivity of photocatalytic oxidation of organic substances. Adv Energy Mater 11(8):2003216
3. Cao X, Han T, Peng Q et al (2020) Modifications of heterogeneous photocatalysts for hydrocarbon C–H bond activation and selective conversion. Chem Commun (Camb) 56(90):13918–13932
4. Yuan B, Zhang B, Wang ZL et al (2017) Photocatalytic aerobic oxidation of toluene and its derivatives to aldehydes on Pd/Bi_2WO_6. Chin J Catal 38(3):440–446
5. Wu HZ, Wang JD, Chen RM et al (2021) Zn-doping mediated formation of oxygen vacancies in SnO_2 with unique electronic structure for efficient and stable photocatalytic toluene degradation. Chin J Catal 42(7):1195–1204
6. Kesavan L, Tiruvalam R, Ab Rahim MH et al (2011) Solvent-free oxidation of primary carbon-hydrogen bonds in toluene using Au–Pd alloy nanoparticles. Science 331(6014):195–199
7. Li XH, Chen JS, Wang XC et al (2011) Metal-free activation of dioxygen by graphene/g-C_3N_4 nanocomposites: functional dyads for selective oxidation of saturated hydrocarbons. J Am Chem Soc 133(21):8074–8077
8. Zhou JC, Yang XF, Wang YQ et al (2014) An efficient oxidation of cyclohexane over Au@TiO_2/MCM-41 catalyst prepared by photocatalytic reduction method using molecular oxygen as oxidant. Catal Commun 46:228–233
9. Su KY, Liu HF, Zeng B et al (2020) Visible-light-driven selective oxidation of toluene into benzaldehyde over nitrogen-modified Nb_2O_5 nanomeshes. ACS Catal 10(2):1324–1333
10. Zhang C, Huang Z, Lu J et al (2018) Generation and confinement of long-lived N-oxyl radical and its photocatalysis. J Am Chem Soc 140(6):2032–2035
11. Liu Y, Chen L, Yuan Q et al (2016) A green and efficient photocatalytic route for the highly-selective oxidation of saturated alpha-carbon C–H bonds in aromatic alkanes over flower-like Bi_2WO_6. Chem Commun (Camb) 52(6):1274–1277
12. Teramura K, Tanaka T, Hosokawa T et al (2004) Selective photooxidation of various hydrocarbons in the liquid phase over V_2O_5/Al_2O_3. Catal Today 96(4):205–209
13. Montini T, Gombac V, Sordelli L et al (2011) Nanostructured Cu/TiO_2 photocatalysts for H_2 production from ethanol and glycerol aqueous solutions. ChemCatChem 3(3):574–577
14. Abe R, Shinmei K, Koumura N et al (2013) Visible-light-induced water splitting based on two-step photoexcitation between

dye-sensitized layered niobate and tungsten oxide photocatalysts in the presence of a triiodide/iodide shuttle redox mediator. J Am Chem Soc 135(45):16872–16884
15. Abe R, Takami H, Murakami N et al (2008) Pristine simple oxides as visible light driven photocatalysts: highly efficient decomposition of organic compounds over platinum-loaded tungsten oxide. J Am Chem Soc 130(25):7780–7781
16. Higashi M, Domen K, Abe R (2013) Fabrication of an efficient $BaTaO_2N$ photoanode harvesting a wide range of visible light for water splitting. J Am Chem Soc 135(28):10238–10241
17. Gombac V, Sordelli L, Montini T et al (2010) CuO_x–TiO_2 photocatalysts for H_2 production from ethanol and glycerol solutions. J Phys Chem A 114(11):3916–3925
18. Zhang YH, Zhang N, Tang ZR et al (2012) Transforming CdS into an efficient visible light photocatalyst for selective oxidation of saturated primary C–H bonds under ambient conditions. Chem Sci 3(9):2812–2822
19. Yang MQ, Zhang Y, Zhang N et al (2013) Visible-light-driven oxidation of primary C–H bonds over CdS with dual co-catalysts graphene and TiO_2. Sci Rep 3:3314
20. Furukawa S, Shishido T, Teramura K et al (2011) Reaction mechanism of selective photooxidation of hydrocarbons over Nb_2O_5. J Phys Chem C 115(39):19320–19327
21. Du P, Moulijn JA, Mul G (2006) Selective photo(catalytic)-oxidation of cyclohexane: effect of wavelength and TiO_2 structure on product yields. J Catal 238(2):342–352
22. Almeida AR, Moulijn JA, Mul G (2008) In situ ATR-FTIR study on the selective photo-oxidation of cyclohexane over anatase TiO_2. J Phys Chem C 112(5):1552–1561
23. Carneiro JT, Yang CC, Moulijn JA et al (2011) The effect of water on the performance of TiO_2 in photocatalytic selective alkane oxidation. J Catal 277(2):129–133
24. Qi KZ, Liu SY, Qiu M (2018) Photocatalytic performance of TiO_2 nanocrystals with/without oxygen defects. Chin J Catal 39(4):867–875
25. Yu JG, Jimmy CY (2010) Low temperature solvent evaporation-induced crystallization synthesis of nanocrystalline TiO_2 photocatalyst. Chin J Chem 21(8):994–997
26. Tripathy J, Lee K, Schmuki P (2014) Tuning the selectivity of photocatalytic synthetic reactions using modified TiO_2 nanotubes. Angew Chem Int Ed Engl 53(46):12605–12608
27. Asahi R (2001) Visible-light photocatalysis in nitrogen-doped titanium oxides. Science 293(5528):269–271
28. Sarina S, Zhu HY, Zheng ZF et al (2012) Driving selective aerobic oxidation of alkyl aromatics by sunlight on alcohol grafted metal hydroxides. Chem Sci 3(6):2138–2146
29. Ide Y, Kawamoto N, Bando Y et al (2013) Ternary modified TiO_2 as a simple and efficient photocatalyst for green organic synthesis. Chem Commun 49(35):3652
30. Song LN, Ding F, Yang YK et al (2018) Synthesis of TiO_2/Bi_2MoO_6 composite for partial oxidation of aromatic alkanes under visible-light illumination. ACS Sustain Chem Eng 6(12):17044–17050
31. Yuan RS, Fan SL, Zhou HX et al (2013) Chlorine-radical-mediated photocatalytic activation of C–H bonds with visible light. Angew Chem Int Ed 52(3):1035–1039
32. Tsai CC, Teng H (2004) Regulation of the physical characteristics of titania nanotube aggregates synthesized from hydrothermal treatment. Chem Mater 16(22):4352–4358
33. Xing M, Zhang J, Chen F et al (2011) An economic method to prepare vacuum activated photocatalysts with high photo-activities and photosensitivities. Chem Commun (Camb) 47(17):4947–4949
34. Lynch J, Giannini C, Cooper JK et al (2015) Substitutional or interstitial site-selective nitrogen doping in TiO_2 nanostructures. J Phys Chem C 119(13):7443–7452
35. Di Valentin C, Finazzi E, Pacchioni G et al (2007) N-doped TiO_2: theory and experiment. Chem Phys 339(1–3):44–56
36. Livraghi S, Chierotti MR, Giamello E et al (2008) Nitrogen-doped titanium dioxide active in photocatalytic reactions with visible light: a multi-technique characterization of differently prepared materials. J Phys Chem C 112(44):17244–17252
37. Livraghi S, Paganini MC, Giamello E et al (2006) Origin of photoactivity of nitrogen-doped titanium dioxide under visible light. J Am Chem Soc 128(49):15666–15671
38. Jiang Z, Yang F, Luo N et al (2008) Solvothermal synthesis of N-doped TiO_2 nanotubes for visible-light-responsive photocatalysis. Chem Commun (Camb) 47:6372–6374
39. Tebben L, Studer A (2011) Nitroxides: applications in synthesis and in polymer chemistry. Angew Chem Int Ed Engl 50(22):5034–5068

Feng Wang received his B.Sc. from Zhengzhou University in 1999 and Ph.D. from Dalian Institute of Chemical Physics (DICP), Chinese Academy of Sciences in 2005. He worked as a postdoctoral researcher at the University of California at Berkeley in USA (2005–006) and at the Catalysis Research Center of Hokkaido University in Japan (2006–009). He serves as a full professor and an independent PI at DICP in 2009, a joint professor in the State Key Laboratory of Catalysis at DICP in 2013, and is the director of the Division of Biomass Conversion & Bio-Energy at DICP since 2018. His current research focuses on the heterogeneous catalysis and biomass conversion.